Enhancing the outcoupling efficiency of quantum dot LEDs with internal nano-scattering pattern

Haowen Liang,[1,2] Ruidong Zhu,[2] Yajie Dong,[2,3] Shin-Tson Wu,[2,*] Juntao Li,[1] Jiahui Wang,[1] and Jianying Zhou[1]

[1]*State Key Laboratory of Optoelectronic Materials and Technologies, Sun Yat-sen University, Guangzhou 510275, China*
[2]*College of Optics and Photonics, University of Central Florida, Orlando, Florida 32816, USA*
[3]*Nano Science Technology Center, University of Central Florida, Orlando, Florida 32826, USA*
[*]*swu@ucf.edu*

Abstract: We report an effective method to extract light from quantum-dot light emitting diodes (QLEDs) by embedding an internal nano-scattering pattern structure. We use finite-difference time-domain method to analyze the light extraction efficiency of red QLEDs with periodic, quasi-random, and random internal nano-scattering pattern structures. Our simulation results indicate that random internal nano-scattering pattern can greatly enhance the outcoupling efficiency while keeping wide viewing angle for the red QLED. Similar results are obtained by extending this approach to green and blue QLEDs. With the proposed red, green, and blue QLEDs combination, we achieve 105.1% Rec. 2020 color gamut in CIE 1976 color space. We demonstrate that internal nano-scattering pattern structures are attractive for display applications, especially for enhancing the outcoupling efficiency of blue QLEDs.

References and links

1. A. P. Alivisatos, "Semiconductor clusters, nanocrystals, and quantum dots," Science **271**(5251), 933–937 (1996).
2. C. B. Murray, D. J. Norris, and M. G. Bawendi, "Synthesis and characterization of nearly monodisperse CdE (E = sulfur, selenium, tellurium) semiconductor nanocrystallites," J. Am. Chem. Soc. **115**(19), 8706–8715 (1993).
3. K. Bourzac, "Quantum dots go on display," Nature **493**(7432), 283 (2013).
4. Y. Shirasaki, G. J. Supran, M. G. Bawendi, and V. Bulović, "Emergence of colloidal quantum-dot light-emitting technologies," Nat. Photonics **38**(09), 703–711 (2013).
5. Z. Luo, D. Xu, and S. T. Wu, "Emerging quantum-dots-enhanced LCDs," J. Disp. Technol. **10**(7), 526–539 (2014).
6. J. Chen, V. Hardev, J. Hartlove, J. Hofler, and E. Lee, "A high-efficiency wide-color-gamut solid-state backlight system for LCDs using quantum dot enhancement film," SID Symp. Dig. Tech. Pap. **43**(1), 895–896 (2012).
7. S. Coe-Sullivan, W. Liu, P. Allen, and J. S. Steckel, "Quantum dots for LED downconversion in display applications," ECS J. Solid State Sci. Technol. **2**(2), R3026–R3030 (2013).
8. J. F. Van Derlofske, J. M. Hillis, A. Lathrop, J. Wheatley, J. Thielen, and G. Benoit, "Illuminating the value of larger color gamuts for quantum dot displays," SID Symp. Dig. Tech. Pap. **45**(1), 237–240 (2014).
9. Z. Luo, Y. Chen, and S. T. Wu, "Wide color gamut LCD with a quantum dot backlight," Opt. Express **21**(22), 26269–26284 (2013).
10. B. S. Mashford, M. Stevenson, Z. Popovic, C. Hamilton, Z. Zhou, C. Breen, J. Steckel, V. Bulovic, M. Bawendi, S. Coe-Sullivan, and P. T. Kazlas, "High-efficiency quantum-dot light-emitting devices with enhanced charge injection," Nat. Photonics **7**(5), 407–412 (2013).
11. H.-M. Kim, A. R. Mohd Yusoff, T.-W. Kim, Y.-G. Seol, H.-P. Kim, and J. Jang, "Semi-transparent quantum-dot light emitting diodes with an inverted structure," J. Mater. Chem. C **2**(12), 2259–2265 (2014).
12. J. Kwak, W. K. Bae, D. Lee, I. Park, J. Lim, M. Park, H. Cho, H. Woo, Y. Yoon, K. Char, S. Lee, and C. Lee, "Bright and efficient full-color colloidal quantum dot light-emitting diodes using an inverted device structure," Nano Lett. **12**(5), 2362–2366 (2012).

13. P. O. Anikeeva, J. E. Halpert, M. G. Bawendi, and V. Bulović, "Electroluminescence from a mixed red-green-blue colloidal quantum dot monolayer," Nano Lett. **7**(8), 2196–2200 (2007).
14. R. Meerheim, M. Furno, S. Hofmann, B. Lüssem, and K. Leo, "Quantification of energy loss mechanisms in organic light-emitting diodes," Appl. Phys. Lett. **97**(25), 253305 (2010).
15. W. Brütting, J. Frischeisen, T. D. Schmidt, B. J. Scholz, and C. Mayr, "Device efficiency of organic light-emitting diodes: Progress by improved light outcoupling," Phys. Status Solidi A **210**(1), 44–65 (2012).
16. N. A. Reinke, C. Ackermann, and W. Brütting, "Light extraction via leaky modes in organic light emitting devices," Opt. Commun. **266**(1), 191–197 (2006).
17. R. Zhu, Z. Luo, and S. T. Wu, "Light extraction analysis and enhancement in a quantum dot light emitting diode," Opt. Express **22**(S7 Suppl 7), A1783–A1798 (2014).
18. Y. Lee, S. Kim, J. Huh, G. Kim, Y. Lee, S. Cho, Y. Kim, and Y. Do, "A high-extraction-efficiency nanopatterned organic light-emitting diode," Appl. Phys. Lett. **82**(21), 3779 (2003).
19. Y. Kim, S. Cho, Y. Song, Y. Lee, Y. Lee, and Y. Do, "Planarized SiN$_x$/spin-on-glass photonic crystal organic light-emitting diodes," Appl. Phys. Lett. **89**(17), 173502 (2006).
20. Y. Do, Y. Kim, Y. Song, and Y. Lee, "Enhanced light extraction efficiency from organic light emitting diodes by insertion of a two-dimensional photonic crystal structure," J. Appl. Phys. **96**(12), 7629 (2004).
21. X. Yang, K. Dev, J. Wang, E. Mutlugun, C. Dang, Y. Zhao, S. Liu, Y. Tang, S. T. Tan, X. W. Sun, and H. V. Demir, "Light extraction efficiency enhancement of colloidal quantum dot light-emitting diodes using large-scale nanopillar arrays," Adv. Funct. Mater. **24**(38), 5977–5984 (2014).
22. International Telecommunication Union, "Parameter values for ultra-high definition television systems for production and international programme exchange," Recommendation ITU-R BT. 2020 (2012).
23. X. Dai, Z. Zhang, Y. Jin, Y. Niu, H. Cao, X. Liang, L. Chen, J. Wang, and X. Peng, "Solution-processed, high-performance light-emitting diodes based on quantum dots," Nature **515**(7525), 96–99 (2014).
24. L. Qian, Y. Zheng, J. Xue, and P. H. Holloway, "Stable and efficient quantum-dot light-emitting diodes based on solution-processed multilayer structures," Nat. Photonics **5**(9), 543–548 (2011).
25. K. A. Neyts, "Simulation of light emission from thin-film microcavities," J. Opt. Soc. Am. A **15**(4), 962–971 (1998).
26. T. D. Schmidt, B. J. Scholz, C. Mayr, and W. Brütting, "Efficiency analysis of organic light-emitting diodes based on optical simulations," IEEE J. Sel. Top. Quantum Electron. **19**(5), 7800412 (2013).
27. D. C. O'shea, T. J. Suleski, A. D. Kathman, and D. W. Prather, *Diffractive Optics Design, Fabrication, and Test* (SPIE Press, 2004).
28. W. H. Koo, S. M. Jeong, F. Araoka, K. Ishikawa, S. Nishimura, T. Toyooka, and H. Takezoe, "Light extraction from organic light-emitting diodes enhanced by spontaneously formed buckles," Nat. Photonics **4**(4), 222–226 (2010).
29. J. H. Jang and M. C. Oh, "Outcoupling enhancement of OLEDs with a randomly distributed ITO pattern fabricated by maskless wet etching method," J. Disp. Technol. **9**(11), 900–903 (2013).
30. J. W. Kim, J. H. Jang, M. C. Oh, J. W. Shin, D. H. Cho, J. H. Moon, and J. I. Lee, "FDTD analysis of the light extraction efficiency of OLEDs with a random scattering layer," Opt. Express **22**(1), 498–507 (2014).
31. E. R. Martins, J. Li, Y. Liu, J. Zhou, and T. F. Krauss, "Engineering gratings for light trapping in photovoltaics: The supercell concept," Phys. Rev. B **86**(4), 041404 (2012).
32. Z. Yu, A. Raman, and S. Fan, "Fundamental limit of light trapping in grating structures," Opt. Express **18**(S3), A366–A380 (2010).
33. J. W. Shin, D. H. Cho, J. Moon, C. W. Joo, J. Lee, J. W. Huh, S. K. Park, J. H. Han, N. S. Cho, J. Hwang, H. Y. Chu, and J. I. Lee, "Random nanostructure scattering layer for suppression of microcavity effect and light extraction in OLEDs," Opt. Lett. **39**(12), 3527–3530 (2014).
34. K. H. Lee, J. H. Lee, H. D. Kang, B. Park, Y. Kwon, H. Ko, C. Lee, J. Lee, and H. Yang, "Over 40 cd/A efficient green quantum dot electroluminescent device comprising uniquely large-sized quantum dots," ACS Nano **8**(5), 4893–4901 (2014).
35. H. Shen, X. Bai, A. Wang, H. Wang, L. Qian, Y. Yang, A. Titove, J. Hyvonen, Y. Zheng, and L. Li, "High-efficient deep-blue light-emitting diodes by using high quality Zn$_x$Cd$_{1-x}$S/ZnS core/shell quantum dots," Adv. Mater. **24**, 2367–2373 (2014).
36. Z. Tan, F. Zhang, T. Zhu, J. Xu, A. Y. Wang, J. D. Dixon, L. Li, Q. Zhang, S. E. Mohney, and J. Ruzyllo, "Bright and color-saturated emission from blue light-emitting diodes based on solution-processed colloidal nanocrystal quantum dots," Nano Lett. **7**(12), 3803–3807 (2007).
37. H. C. Lee, *Introduction to Color Imaging Science* (Cambridge University, 2005).

1. Introduction

Colloidal quantum dots (QDs) exhibit several attractive features, such as high quantum efficiency, tunable emission wavelength through particle size control, and narrow emission bandwidth which leads to vivid colors [1,2]. These properties make QDs attractive for liquid crystal displays (LCDs) [3] and organic light-emitting diodes (OLEDs) [4] to provide reliable and saturated red, green, and blue (RGB) primaries, which form a large color gamut for next generation displays.

Photoluminescence (PL) and electroluminescence (EL) are two common QD operation mechanisms. PL-type QDs have been integrated into LCD backlight to provide vivid colors and ~15% increased optical efficiency [5]. In quantum dots enhancement films (QDEFs), red and green QDs are dispersed in the plastic film and tuning the size of QDs to create right wavelength [6]. The red/green QDs are excited by the blue LED to emit pure red and green lights. Several companies including Nanosys [6], QD vision [7], 3M [8] and Nanoco/Dow are actively engaging in this promising technology. It is reported that 115% color gamut in CIE1931 and 140% in CIE1976 color space can be achieved with QDEFs [9]. In 2013, Sony announced first commercial Triluminos LCD TVs [3] and Amazon rolled out Kindle Fire tablets, and in 2015 both LG and Samsung exhibited QD-enhanced LCDs.

At current stage, EL-type quantum dot light-emitting diodes (QLEDs) [10,11] remain inferior to organic light-emitting diodes (OLEDs) in terms of brightness and efficiency. Replacing the organic emitting layer by QDs, QLEDs generate Gaussian-like emission spectra with a full width at half maximum (FWHM) below 30nm [12,13], which shows more saturated colors than a typical OLED (FWHM~100nm) [14]. However, the light output is influenced by the external quantum efficiency (EQE). The outcoupling efficiency is constrained by the ~20% ceiling of the total radiated power [14–16]. Therefore, enhancing the light extraction of QLED structures plays an important role in the application for QLEDs. Recent result shows that by combining a high refractive index substrate with macroextractors, the light outcoupling efficiency can be doubled [17]. This method is acceptable for QLED as illuminator, in which the pixel size is large. But for a high resolution display, the pixel size is around ~100μm for TVs and monitors, and ~50μm for smart phones. It is challenging to assemble macroextractors onto these high resolution devices. Another method to enhance outcoupling efficiency is to integrate internal nano-scattering pattern in light-emitting devices [18–20]. The first study offering detailed insight into the light extraction efficiency enhancement of QLED devices came out recently by introducing large-scale nanopillar arrays on the surface of glass substrate [21]. This approach opens up a new window to improve the optical performances of OLEDs with small pixel sizes. However, a panoramic analysis of light extraction from QLED with various internal nano-scattering patterns is still lacking.

In this paper, we first utilize the dipole model to analyze the amount of power coupled to different optical channels for a typical red QLED. The optimal pattern style can be selected from among periodic, quasi-random, and random internal nano-scattering patterns by systematically analyzing the outcoupling efficiency as well as the radiated pattern of a patterned QLED. Next, we extend this approach to green and blue QLEDs and then compare the obtained color gamut in both CIE1976 and CIE1931 for the patterned and non-patterned QLEDs with that proposed by ITU-R Recommendation BT.2020, namely Rec. 2020, for ultra-high definition televisions [22]. This analysis demonstrates the feasibility of QLED display with internal nano-scattering pattern.

2. Power dissipation analysis

There are two types of QLED structure: forward configuration and inverted configuration. In the forward structure, the upper metal layer performs as the cathode and the ITO works as the anode, while it is inverted in the inverted configuration. So far, there is no certain conclusion on which type is superior. It is easy to implement solution-process to fabricate devices with forward structure [23], while inverted QLEDs are easier to be embedded in n-type TFT backplanes [12]. Here we use the red QLED with forward structure as an example to analyze the power dissipation issue; the method is also applicable to the inverted configuration.

Figure 1(a) depicts a typical forward structure of a red QLED [24]. It consists of layers of ITO (indium-tin-oxide) cathode (25nm)/ poly (ethylenedioxythiophene):polystyrene sulphonate (PEDOT:PSS) hold-injection layer (40nm)/ poly[9, 9-dioctylfluorene-co-N-[4-(3-methylpropyl)]-diphenylamine] (TFB) (30nm)/ CdSe-CdS (cadmium selenide-cadmium sulfide)core-shell QD layer (30nm)/ ZnO nano-particles (25nm)/ /Aluminum anode (100nm).

The PL spectrum of the reported QDs is shown in Fig. 1(b). The central wavelength is 640nm with FWHM~27nm, quantum yield >90%, and outstanding optical properties [23]
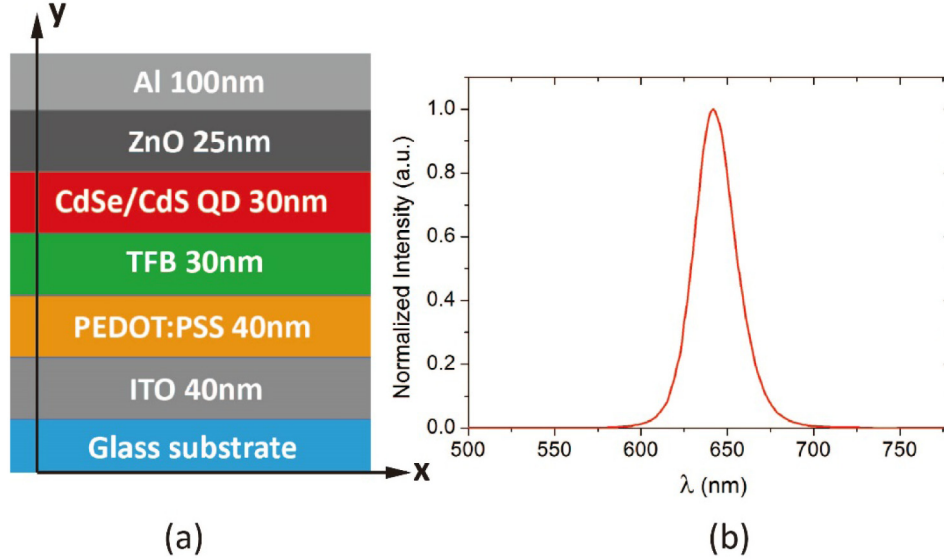

Fig. 1. (a) A typical structure of red QLED and (b) PL spectrum of the reported red QDs.

Here, we apply the rigorous dipole model to investigate the power dissipation within an infinite multilayer medium [25]. In this model, the multilayer structure is simplified to a three-layer structure and the quantum dots are considered as isotropic emitters. The external quantum efficiency (EQE) of the QLEDs can be expressed as:

$$EQE = \eta IQE = \eta \gamma q_{eff},\qquad(1)$$

where η is the outcoupling efficiency and IQE is the internal quantum efficiency. The IQE is tightly related to the effective quantum yield q_{eff} which is close to the quantum yield q of the quantum dots and the charge carrier balance factor γ ($\gamma = 1$ for the ideal case). The power generated by dipoles within a three-layer structure normalized to the power emitted in an infinite medium is given by [26]:

$$P = 1 - q + qF = 1 - q + q \int_{\lambda_1}^{\lambda_2} S(\lambda) \int_0^\infty K(k_x) dk_x d\lambda,\qquad(2)$$

where F is the Purcell factor, $S(\lambda)$ is the normalized PL spectra of QDs, $K(k_x)$ is the power dissipation density regarding the in-plane wave vector k_x for waves propagating in the emitting layer, and q is related to q_{eff} as:

$$\frac{q_{eff}}{q} = \frac{F}{qF + 1 - q}.\qquad(3)$$

As reported in [23,24], the intrinsic quantum yield q of the QDs is higher than 90%. Here, our main objective is to analyze and optimize the performance of QLEDs with internal nano-scattering pattern in order to improve outcoupling efficiency η. In our simulations, q_{eff} is approximated to be 1.

To analyze the outcoupling efficiency of QLEDs, we write the explicit form of K in Eq. (2) as [26]:

$$K = \frac{1}{3}K_{TMv} + \frac{2}{3}\left(K_{TMh} + K_{TEh}\right). \tag{4}$$

In Eq. (4), v and h represent the parallel and perpendicular power contribution of dipoles respectively; TM and TE stand for the transverse electric and transverse magnetic fields. Each term in Eq. (4) is given explicitly in [17].

The power dissipation spectrum can be divided into four modes: direct emission, substrate mode, waveguide mode, and surface plasmons. Each mode can be sorted out by the in-plane wave vector k_x: 1) Direct emission: $0 < k_x \leq k_0 \cdot n_{air}$. It denotes the amount of light which can leave the QLED; 2) Substrate mode: $k_0 \cdot n_{air} < k_x \leq k_0 \cdot n_{glass}$, which denotes the amount of light trapped in the glass substrate due to total internal reflection (TIR); 3) Waveguide mode: $k_0 \cdot n_{glass} < k_x \leq k_0 \cdot n_{eff}$. The radiation of dipoles in this mode does no longer enter the glass substrate and is wave-guided in the layers between glass substrate and cathode where n_{eff} is the equivalent refractive index of ITO, QDs, and organic layers; 4) Surface plasmons: $k_0 \cdot n_{eff} < k_x$. It denotes the evanescent wave at the organic-ITO interface.

The outcoupling efficiency of this red QLED is evaluated as the proportion of the directly emitted power P_{dir} and total radiated power P_{tol}, i.e., $\eta = P_{dir} / P_{tol}$. Power dissipation in other modes can also be analyzed with the same relationship.
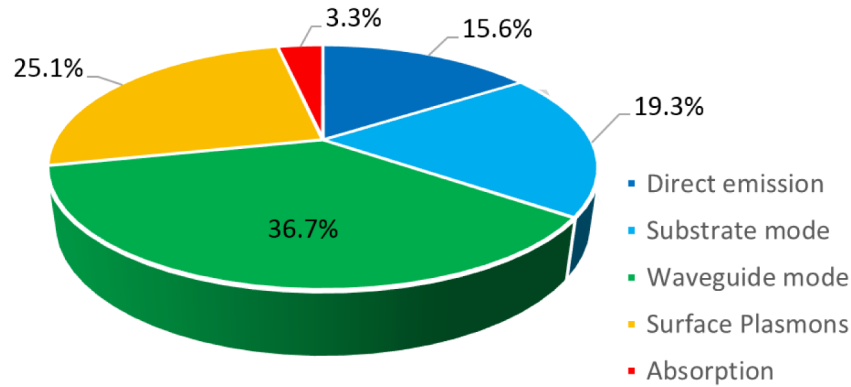

Fig. 2. The ratios of different optical channels for the red QLED.

Figure 2 illustrates the amount of power coupled to different optical channels for our red QLED model. The simulated EQE of the proposed QLED is 15.6% ($\eta \approx EQE$), which is still constrained within the efficiency ceiling ~20%. Moreover, 36.7% of light is trapped in waveguide mode. As reported in [17], the outcoupling efficiency can be doubled by using high index substrates and macroextractors. This benefits the QLEDs for illumination, but the macroextractors are too large for high resolution density displays. In contrast, our proposed internal nano-scattering pattern has two advantages for QLED displays: 1) Its dimension is small enough to accommodate small (~50μm) pixel sizes, and 2) it can effectively extract light in waveguide mode. We will give detailed analysis in the following section.

3. Structure design

The internal nano-scattering pattern is inserted between the glass substrate and ITO electrode. Silicon-Nitride (SiN$_x$) is commonly utilized as the material of rods in nano-scattering pattern because its refractive index ($n_{SiNx} \sim 1.9$) is larger than that of ITO ($n_{ITO} \sim 1.8$). By backfilling the nano-scattering pattern with Silicon Dioxide (SiO$_2$) of 200nm, the nano-scattering pattern is formed and has the ability to diffract electromagnetic wave with specific wavelengths in series of diffracted orders. According to Fermat's principle, light tends to propagate in the material with higher refractive index in a waveguide; therefore a coating layer with high index on ITO can further extract light from organic layers. Here we use SiN$_x$ of 20nm as the

over-coating layer. Similar structure is validated in [19] and the red QLED with internal nano-scattering pattern is illustrated in Fig. 3. The diffracted wavelengths and diffracted orders are determined by the heights of the rods d and the pattern parameter a. Generally the scattering follows the diffraction relationship as [27]:

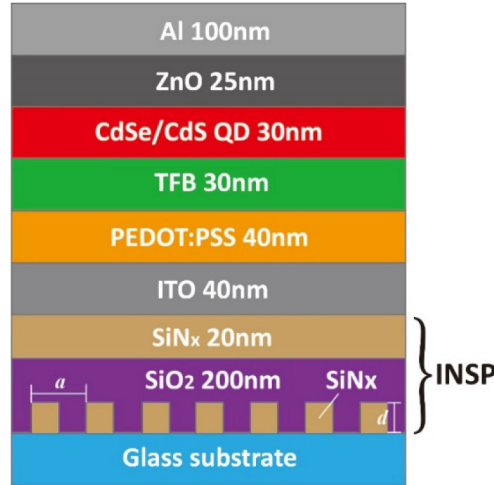$$k_{out} = k_{in} - m\frac{2\pi}{a}, \quad m = 0, \pm 1, \pm 2, ...$$
(5)

Fig. 3. Red QLED with internal nano-scattering pattern.

Various types of internal nano-scattering pattern, including periodic [18–20], quasi-random [28], and random ones [29,30] have shown the ability of light extraction in OLEDs. Similarly, these approaches can be extended to QLEDs. However, as the FWHMs of the PL QD emission spectra are much narrower than those of OLEDs, the performances of these three patterns must be reanalyzed. Here we use FDTD method to compare the pros and cons of these three patterns.

Commonly FDTD simulations should be carried out for three dimensions. In the 3D model, the dipoles are oriented parallel and perpendicular to the QLED layers. In order to study the physical insights of the device while reducing the required amount of simulation time and memory, a 3D structure with reflection symmetry and rotational symmetry can be simplified to a 2D model. In the 3D case the nano-scattering pattern appears in the form of nano-pillar array. Here the periodic and quasi-random cases possess reflection symmetry so that the models can be simplified to 2D along the axis of symmetry; meanwhile the random case can be understood as a periodic structure with infinite period, which can also be reduced to 2D model by rotational symmetry [31]. Thus, the 2D simulations can be justified.

In the model the horizontal scale (x) must be much larger than the vertical scale (y) to make it almost infinite. We choose x = 50μm for each layer so that it is much larger than the thickness of layers (about tens nanometers).

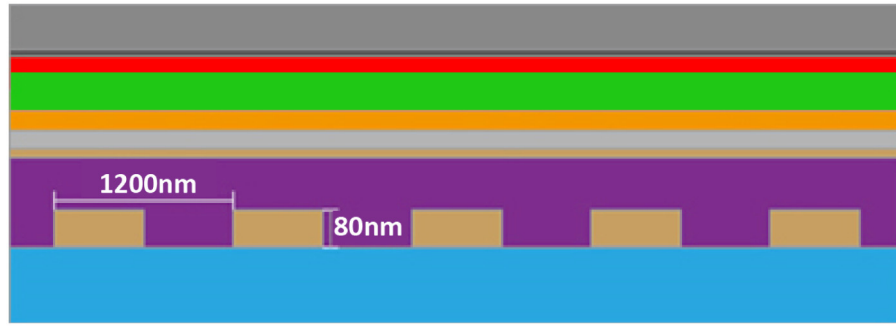## 3.1 Periodic internal nano-scattering pattern

Fig. 4. Schematic diagram of periodic internal nano-scattering pattern s for red QLEDs: pattern parameter of 1200nm and height of 80nm

Figure 4 illustrates the structure of periodic internal nano-scattering pattern. The height (d) of the SiN$_x$ pattern is 80nm, which is obtained by tuning d with an interval of 10nm from 60nm to 100nm to couple the largest amount of light in the wavelength region around 640nm. The outcoupling efficiency enhancements are reduced in absolute terms by 5.2%, 2.7%, 1.6% and 3.8% for d = 60nm, 70nm, 90nm and 100nm relative to the optimal height d = 80nm of this layer. Because the emission bandwidth of QLEDs is narrow, a large amount of light can be effectively scattered by the periodic internal nano-scattering pattern. Therefore, this periodic pattern exhibits excellent ability to extract the trapped light. Figure 5 depicts the angular radiated pattern of a red QLED with and without periodic internal nano-scattering pattern. We achieve a 2.14X on-axial enhancement and 1.65X outcoupling efficiency by integrating over the viewing angle ± 90°. However, the radiated pattern is strongly angular dependent; as noted in Eq. (5) only the k_{in} corresponding to low orders ($|m| \approx 2[a/\lambda] + 1$) [32] can be extracted from the QLED with periodic pattern. Figure 5 shows that the FWHM is reduced to ± 35° from the original value of ± 59°. This viewing angle narrowing effect would strongly limit the utilization of patterned QLED in display, especially for TVs and monitors.
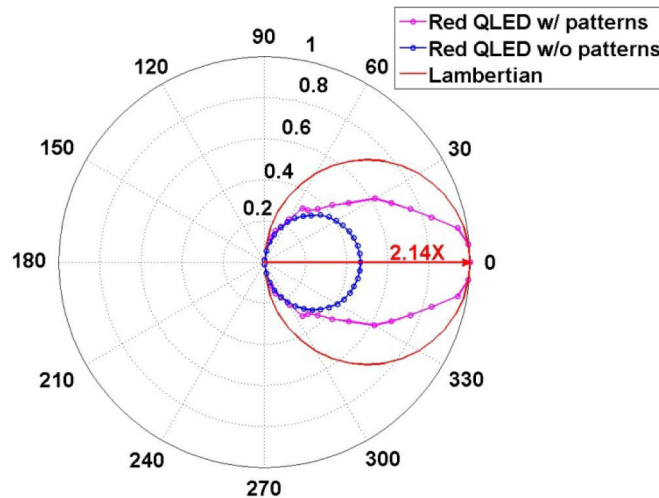

Fig. 5. Simulated angular radiated patterns of red QLED with and without periodic internal nano-scattering pattern.
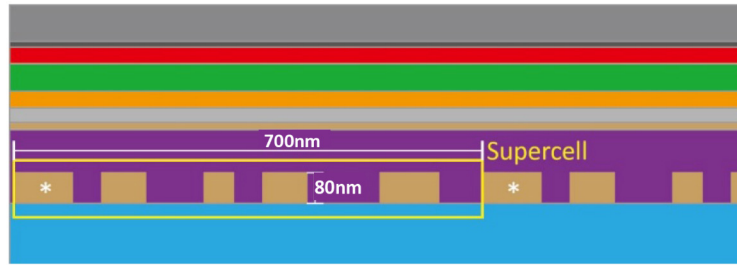
3.2 Quasi-random internal nano-scattering pattern

Fig. 6. Schematic diagram of quasi-random internal nano-scattering pattern for red QLEDs: the period of the supercell is 700nm, while the height of the nano-rods is 80nm.

A quasi-random structure is based on the idea of supercell: a large unit cell containing fine structures [31], as shown in Fig. 6. The advantages to utilize quasi-random internal nano-scattering pattern to extract light from light emitting devices are twofold: 1) the periodicity of the quasi-random internal nano-scattering pattern determine a specific wavelength around which light can be extracted effectively; 2) the randomness of a supercell can open up a broader parameter-space while maintaining control over the diffracted orders. The fine-design of the supercell is used to balance the above two factors.

The nano-patterns in a supercell are spatially offset from one another, which imposes a phase shift between the diffraction orders. This phase shift is used to design destructive interference for the lower orders and constructive interference for the higher orders. In this case, rather than only extracting low diffracted orders ($|m| \leq 3$) from the QLED, the quasi-random internal nano-scattering pattern suppresses the ± 1, ± 2 diffracted orders and enhance the high orders of ± 5, ± 6 so that the viewing angle can be expanded. The angular radiated pattern of red QLED with quasi-random internal nano-scattering pattern is illustrated in Fig. 7. Rather than resulting in a severe reduction of FWHM in the angular emission pattern, the quasi-random internal nano-scattering pattern does scatter high diffracted orders in QLEDs and a $\pm 50°$ FWHM is obtained (the original value is $\pm 59°$). However, as lower diffracted orders have been suppressed, light is less effective to be extracted from QLEDs than what is with periodic nano-pattern (an on-axial enhancement of 1.33X and 1.27X outcoupling efficiency by integrating over the emission patterns can be achieved).
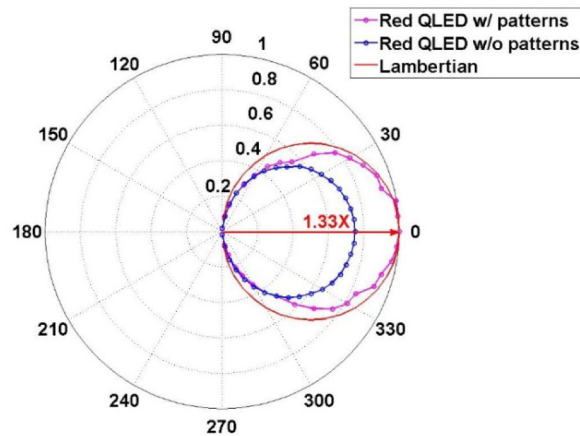

Fig. 7. Simulated angular radiation patterns of red QLED with and without quasi-random internal nano-scattering pattern.
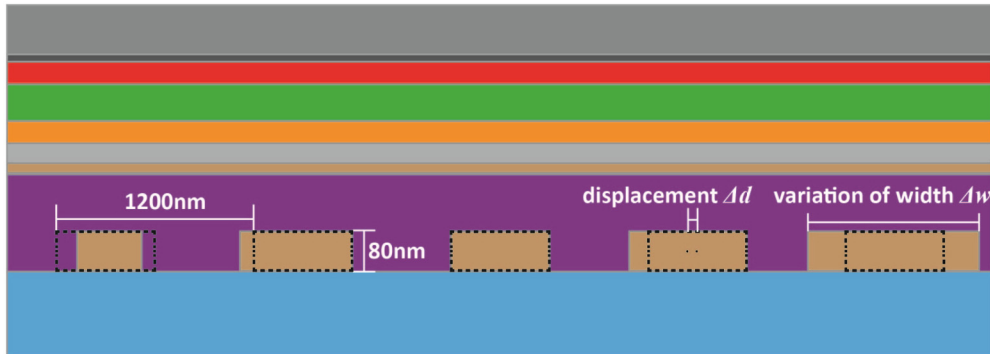
3.3 Random internal nano-scattering pattern

Fig. 8. Schematic diagram of red QLEDs with random internal nano-scattering pattern: pattern parameter = 1200nm and height = 80nm. Both displacement and variation of width characterize the randomness of pattern.

A random internal nano-scattering pattern consists of nano-rods with random positions and sizes as it has the probability to overcome the spectral shift and angular dependence of the output light and thus be adopted in commercial OLEDs [30]. The randomness of nano-rods can be characterized by two parameters: Δd which denotes the central displacement of a nano-rod from the position of periodic case, and Δw which tells the variation of width of nano-rods. Figure 8 depicts the structure of random internal nano-scattering pattern.

In the case of OLED (especially white OLED), it is expected that random internal nano-scattering pattern with large randomness has the light extraction effect without wavelength dependency because of the wide FWHM (~100nm) of OLED spectra [33]; while the randomness for patterned QLEDs ought not to be too large due to the narrow PL spectrum (~30nm) of QDs. As Δd influences the pattern parameter which results in lowering the extracting ability of the internal nano-scattering pattern while Δw excites higher diffracted orders, Δd should be kept small while Δw can be a large value.

In our simulation, we use $\Delta d = \pm 200nm$ and $\Delta w = \pm 800nm$ (SET I) in the red QLED model. As plotted in Fig. 9(a), we obtain an on-axis enhancement of 1.55X and 1.53X in outcoupling efficiency. The viewing angle of the patterned QLED reaches $\pm 52°$ because the variation of the width of nano-rods excites higher orders and more amount of light with larger k_x can be extracted from waveguide mode. To verify whether this combination is acceptable, we compare the outcoupling efficiency with larger Δd ($\Delta d = \pm 500nm$, $\Delta w = \pm 800nm$, SET II) and larger Δw ($\Delta d = \pm 200nm$, $\Delta w = \pm 1200nm$, SET III) in Fig. 9(b). The outcoupling efficiencies of SET II and SET III are 1.16X and 1.50X, respectively.
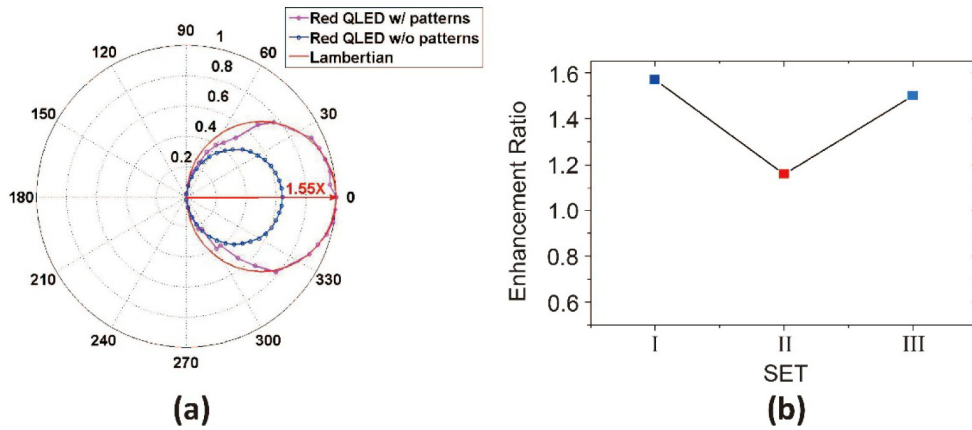
Fig. 9. (a) Angular radiated patterns of red QLED with and without random internal nano-scattering pattern, and (b) enhancement ratio of patterned QLEDs with different randomness.

Figure 10 shows the luminance distribution for the purpose of display applications. By considering both outcoupling efficiency and viewing angle, the approach of random internal nano-scattering pattern is effective to QLED light extraction. Actually, Δd and Δw would be automatically introduced into periodic pattern during manufacturing [21].
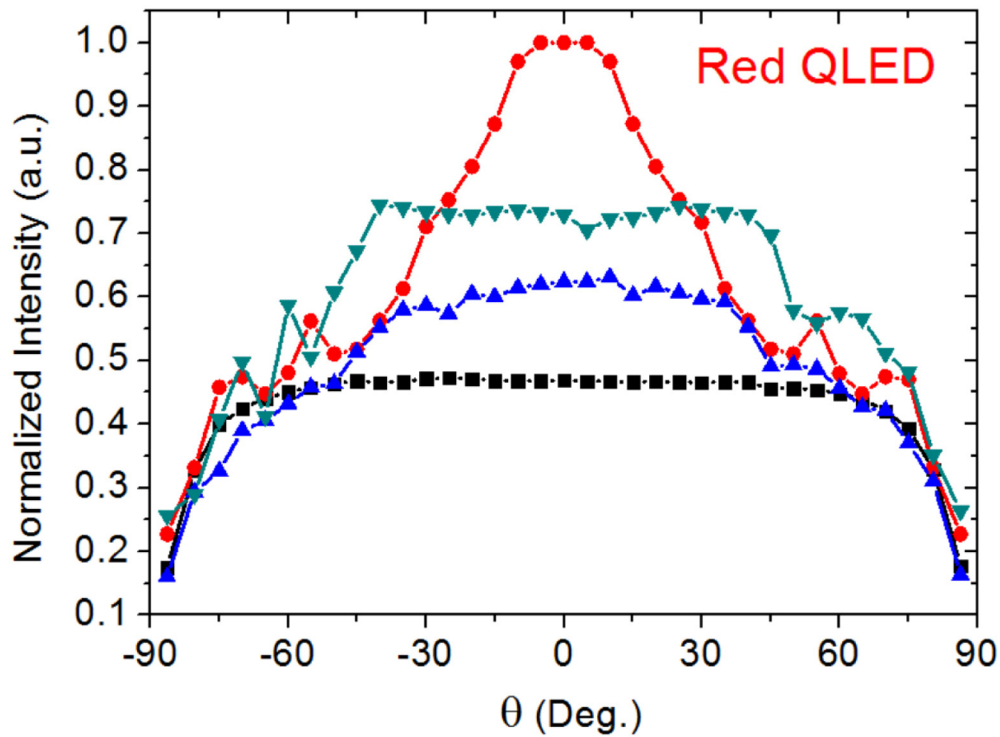

Fig. 10. Normalized luminance distribution of red QLED without (black line) and with periodic (red line), quasi-random (blue line), and random (cyan line) internal nano-scattering patterns.

Finally the polarization of the light outcoupled from the patterned QLEDs is also given. For periodic and quasi-random cases, the emission pattern repeats along the axis of

symmetry. Therefore the outcoupling efficiency is at maximum along the axis of symmetry and is reduced at any other directions. This effect leads to polarization in the orientation along the axis of symmetry. As random structure can be regarded as periodic structure with infinite period, it possesses rotational symmetry and the outcoupling efficiency is identical toward any orientations. Therefore, random structure will not affect the polarization of the light outcoupled from QLED.

4. RGB QLED with random internal nano-scattering pattern and color gamut

The design of internal nano-scattering pattern can be extended to light extraction from green and blue QLEDs. The proposed structure of the green QLED consists of ITO (160nm)/ PEDOT:PSS (20nm)/PVK (20nm)/CdSe@ZnS/ZnS QDs (40 nm)/ZnO nano-particles (50nm)/ Aluminum (100nm) [34] and ITO (40nm)/PEDOT:PSS(40 nm)/TFB(30 nm)/CdS/ZnS core/ shell QD(20nm)/ZnO nano-particles (25 nm)/Aluminum (100nm)for the blue QLED [35]. The central wavelength of the PL spectra for the green QD is 516nm with FWHM~21nm [34], while for the blue one is 460nm with FWHM~18nm [36].

Table 1 lists the structural parameters and enhancement ratios of three types of internal nano-scattering pattern for RGB QLEDs. Results show that the three types of pattern produce similar enhancing effect on green and blue QLEDs. Figures 11(a) and 11(b) compare the normalized luminance for different patterned green and blue QLEDs, respectively. Random internal nano-scattering pattern possess the ability to maintain good viewing angle consistent with those of conventional QLEDs ($\pm 45°$ for green and $\pm 45°$ for blue).

Table 1. Structural parameters of internal nano-scattering pattern for RGB QLEDs.

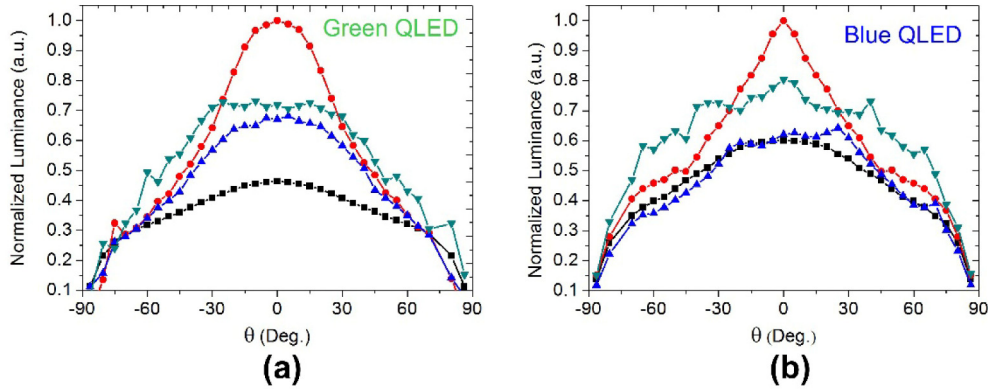| Color	Periodic			Quasi-random			Random		
	a (nm)	d (nm)	η	$a_{supercell}$(nm)	d (nm)	η	Δd(nm)	Δw (nm)	η
Red	1200	80	1.65X	700	80	1.27X	± 200	± 800	1.53X
Green	920	90	1.57X	640	90	1.29X	± 150	± 800	1.38X
Blue	700	110	1.34X	544	110	1.09X	± 110	± 800	1.29X

Fig. 11. Normalized luminance distribution of (a) green QLED and (b) blue QLED without (black line) and with periodic (red line), quasi-random (blue line), and random (cyan line) internal nano-scattering patterns.

Color saturation is an important criterion for display devices. As evidence of this trend, the International Telecommunication Union (ITU) has published recommendations (ITU-R Recommendation BT.2020) for ultra-high definition TVs that include a very large color gamut specification, commonly known as Rec. 2020 [22]. QD is an emerging display technology which can easily and efficiently increase color gamut and provide superior color rendering. In fact, QD is most likely the only production-ready technical solution being able to approximately achieve Rec. 2020 today. Here we use the proposed RGB QLEDs as three

primaries to elucidate its color performance. We present the color gamut in both CIE1976 and CIE1931, as CIE suggests using CIE1976 definition since it is a color uniform space while most display companies are still using CIE 1931 to evaluate their products.

To form the additive mixture of D65 white point (x_W = 0.3127, y_W = 0.3290), the tristimulus values of D65 are matched by unit amounts of the three primaries [37]:

$$D65(aX_r + bX_g + cX_b, aY_r + bY_g + cbY_b, aZ_r + bZ_g + cZ_b) = aR + bG + cB \quad (6)$$

where the chromaticity coordinates of RGB are specified by tristimulus values $R(X_r, Y_r, Z_r)$, $G(X_g, Y_g, Z_g)$ and $B(X_b, Y_b, Z_b)$ and a, b, c are defined by the following relations:

$$\begin{cases} x_w = k_r x_r + k_g x_g + k_b x_b \\ y_w = k_r y_r + k_g y_g + k_b y_b \, , \\ z_w = 1 - x_w - y_w \end{cases} \quad (7)$$

$$\begin{cases} k_r = \dfrac{a(X_r + Y_r + Z_r)}{a(X_r + Y_r + Z_r) + b(X_g + Y_g + Z_g) + c(X_b + Y_b + Z_b)} \\[2ex] k_g = \dfrac{b(X_g + Y_g + Z_g)}{a(X_r + Y_r + Z_r) + b(X_g + Y_g + Z_g) + c(X_b + Y_b + Z_b)} \, . \\[2ex] k_b = \dfrac{c(X_c + Y_c + Z_c)}{a(X_r + Y_r + Z_r) + b(X_g + Y_g + Z_g) + c(X_b + Y_b + Z_b)} \end{cases} \quad (8)$$

Based on our simulation, the mixing coefficients are a = 0.439, b = 0.302, and c = 0.259 for the case without random internal nano-scattering pattern, and a = 0.462, b = 0.300, and c = 0.248 for the case with such pattern. The spectral profile of RGB QLEDs is illustrated in Fig. 12.
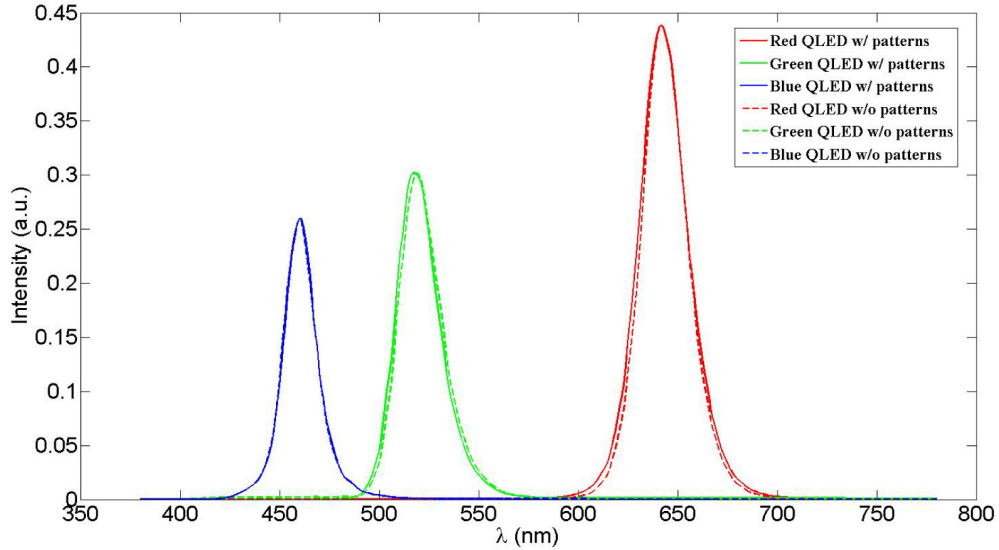

Fig. 12. Spectral profile of RGB primaries for our proposed QLED display.

Figures 13(a) and 13(b) depict the color gamut of Rec. 2020 and QLED display with and without random pattern in CIE1976 and CIE1931 color space, respectively. In general, the color gamut defined by CIE 1976 is much larger than that of CIE 1931. Our simulations show

that the proposed RGB QLED display forms a wide color space in CIE1976 (104.7% Rec. 2020), but it is smaller in CIE1931 (95% Rec. 2020). This is because in CIE 1931 color space, green and cyan colors occupy a very large area, and the color coordinates of green primary affect the color gamut greatly; while in CIE 1976 blue area occupies a large portion and blue primary plays an important role. The large color gamut still maintains after introducing random internal nano-scattering pattern into RGB QLEDs, which covers an area of 105.1% Rec. 2020 in CIE1976 and it is of 98% Rec. 2020 in CIE1931. Thus, random internal nano-scattering pattern would not significantly change the chromatic characteristics of RGB QLED display. As a result, this approach would improve the lifetime and outcoupling efficiency of a QLED display, especially for blue pixels whose lifetime and brightness are still important issues for practical applications.
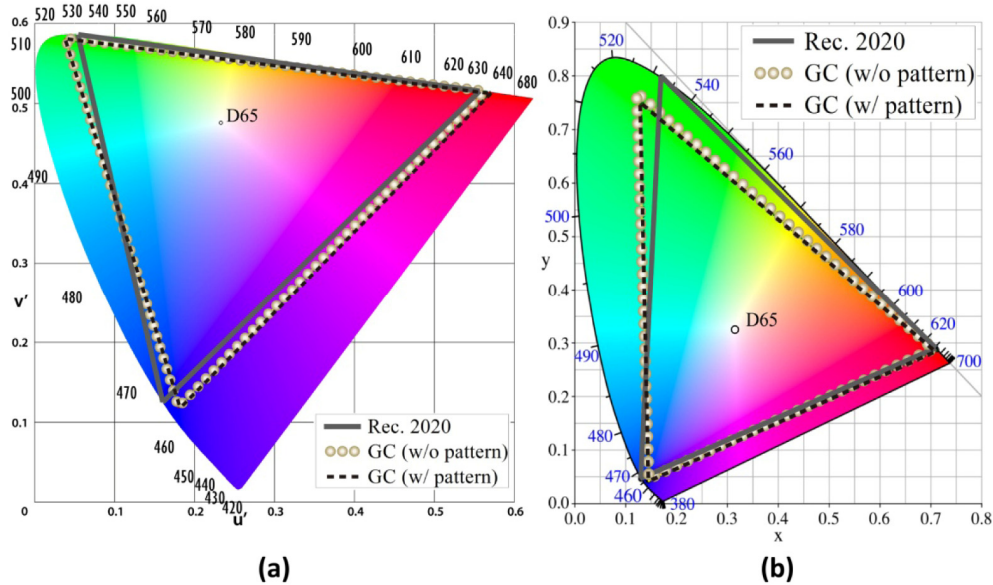

Fig. 13. Color gamut of Rec. 2020 and RGB QLED with and without random internal nano-scattering pattern in (a) CIE1976 and (b) CIE1931.

5. Conclusion

We find that internal nano-scattering pattern can effectively extract light from QLEDs. By comparing the outcoupling efficiency and viewing angle of the red QLED with periodic, quasi-random, and random internal nano-scattering pattern, we find that the random internal nano-scattering pattern is the prominent candidate among these three designs for QLED applications. Similar results are obtained by extrapolating the approach for green and blue QLEDs. Finally, a 105.1% Rec. 2020 color gamut in CIE 1976 is obtained by our patterned RGB QLEDs. We confirm that internal nano-scattering pattern is suitable for display applications, especially to enhance the outcoupling efficiency of blue QLED.